

Project information	
Project full title	EuroSea: Improving and Integrating European Ocean Observing and Forecasting Systems for Sustainable use of the Oceans
Project acronym	<b>EuroSea</b>
Grant agreement number	862626
Project start date and duration	1 November 2019, 50 months
Project website	<a href="https://www.eurosea.eu">https://www.eurosea.eu</a>

Deliverable information	
Deliverable number	5.4
Deliverable title	<b>CMEMS downscaled wave operational forecast system</b>
Description	This document describes the numerical modelling work for waves done in wp5.2. needed to implement OSPAC
Work Package number	WP5
Work Package title	Coastal Resilience and Operational Services Demonstrator
Lead beneficiary	UPC
Lead authors	Manuel Espino (UPC)
Contributors	Ivan Federico (CMCC), Salvatore Causio (CMCC), and Giovanni Coppini (CMCC), Maria Liste (UPC), Marc Mestres (UPC), Agustín S.-Arcilla (UPC), Marcos García Sotillo (EPPE), Manuel García León (EPPE), Enrique Álvarez-Fanjul (EPPE)
Due date	31 October 2021
Submission date	3 November 2021
Comments	This document was submitted 3 days late due to a formal revision.



This project has received funding from the European Union's Horizon 2020 research and innovation programme under grant agreement No. 862626.

## Table of contents

Executive summary.....	1
1. Introduction.....	1
2. Areas of Interest.....	2
2.1. Taranto.....	2
2.2. Barcelona.....	4
3. Methodology.....	5
3.1. Numerical models.....	5
Taranto.....	5
Barcelona.....	6
3.2. Grid generation and bathymetry interpolation.....	7
Taranto.....	7
Barcelona.....	8
3.3. Initial and Lateral boundary conditions. Forcings.....	8
Taranto.....	8
Barcelona.....	8
3.4. Physical and numerical setting.....	9
Taranto.....	9
Barcelona.....	9
3.5. Results.....	10
Taranto.....	10
Barcelona.....	14
References.....	18
References for Taranto subsections.....	18
References for Barcelona subsections.....	19

## Executive summary

This document explain I detail the set-up and implementation of two numerical high-resolution wave models for the test cases of Taranto and Barcelona, as expected in the EuroSea workplan. Both models are state of the art and have been carefully validated. The operating services resulting will be in the core of OSPAC product, the main deliverable of WP5.2.

The third pilot involved in the project, Alexandría, does not have models ready, since this port, quite unexpectedly, failed to obtain the internal required permits to work in the project. Nevertheless, this is not a concerning delay, since all methodologies are developed, and we will proceed to the modelling work once the substitute port is designated. At this moment, locations at Colombia or Madagascar are being studied. Contacts with local authorities are established, and a final decision will be made before the end of 2021

## 1. Introduction

The ocean is an essential part of the planet that plays a crucial role in the global life system and provides vital resources for humanity. Coastal zones are the most affected areas by direct anthropic pressures, and their management is very complex due to the multiple interconnected processes that occur there. Therefore, understanding the physical behavior of coastal zones is vital to managing the main problems related to impacts and resource exploitation activities (Liste et al., 2021). In this coastal setting, ports and adjacent cities are one of the main anthropic infrastructures that generate economic wealth; the increase in maritime traffic has resulted in rapid growth in port activity. As Ports and Cities are affected by met-ocean conditions, especially extreme events, personalized real-time and forecast information on environmental conditions is needed to manage their growth. Wind, waves, and sea level are traditionally the most critical metocean parameters.

Supporting port and city activities requires accurate ocean forecasting systems; In response to this growing demand for continuous and updated met-ocean information, high-resolution models are being implemented in coastal areas, combined with in situ observations, are allowing a better understanding and characterization of the main hydrodynamic characteristics of these areas. As a result, the operational physical oceanography is maturing quickly, and high-resolution wave modelling as an operational capability is now a fact.

In the framework of the EuroSea Project, the WP5 team has been working on developing wave forecasting operational tool with enough resolution to solve the wave dynamics of restricted domains such as Barcelona's and Taranto's local coastal waters, harbors, and beaches. This deliverable provides a complete description of the wave operational forecast systems in Barcelona's and Taranto's local coastal waters.

The report is organized as follows: Section 2 describes the study site. Section 3 describes the 3D modeling systems and setups. Finally, section 4 presents validations and results.

## 2. Areas of Interest

### 2.1. Taranto

The Area of Interest is focused on the Southern Adriatic and Northern Ionian seas of Mediterranean basin, with special zoom in the Gulf of Taranto (hereafter GT) and particularly in the Mar Grande and Mar Piccolo where the port of Taranto is located.

The southern Adriatic Sea extends approximately southward along the latitude of 42°N to the threshold of the Strait of Otranto and has a maximum depth of 1270 m. An exchange of waters with the Ionian Sea occurs at the Strait of Otranto at approximately 40°N. The northern Ionian Sea extends south of 38°N and has a steeper continental slope than the Adriatic basin. The offshore maximum depth is 3500–3700 m.

The GT (Figure 1a) is situated in the northwestern Ionian Sea and is approximately delimited in open sea by the line connecting Apulia and Calabria (Gulf of Taranto – Boundary Section, GT-BS in Figure 1a). It is a deep, semi-enclosed ocean area in southern Italy encircled by two peninsulas, Apulia and Basilicata/Calabria (Figure 1a). It is open to the northern Ionian Sea, and a deep trench of more than 2000 m connects it to the eastern Mediterranean Sea. The continental shelf area, considered as the area from the coasts to the 200 m depth contour, occupies only 10 % of the total Gulf area (Pinardi et al., 2016) with the shelf wider on the Apulia than the Calabria side.

A 7.5 km wide sheltered elliptical embayment, called the Mar Grande – Mar Piccolo system of Taranto, see Figure 1b, hereafter named MG-MP), opens in the northeastern part of the GT. The MG-MP is a marine system experienced over the last few decades strong biochemical pollution and environmental degradation, and it is considered a hotspot study site for economic, ecological and scientific reasons

Few studies are available on the wave climate of the Gulf of Taranto. Greco and Martino (2014) evaluated the main direction of the wave field off the Ionian western coast, performed by means of hindcasting method. The frequency of the sea state from SE direction is higher than 50%. Damiani et al. (2007) described the wave climate for the year 2006 using a buoy in proximity of the mouth of the Great Sea in Taranto. The buoy was moored about 1.5 km from Taranto at a location with a water depth of about 72 m, to measure sea states not altered by the interaction with bottom. They reported that the longest fetch is about 1400 km from the SSE. The recorded wave heights during the year analyzed were relatively small and the maximum significant wave height was  $H_s = 2.88\text{m}$  (April 2006). The wave climate in the Gulf is characterized by a rather constant SSE direction. The waves come from a quite limited approaching sector and the wave field direction is very constant overall the year. The only remarkable change happens during the summer season when there is a greater occurrence of low height waves generated from local winds blowing from NW directions (Figure 2).

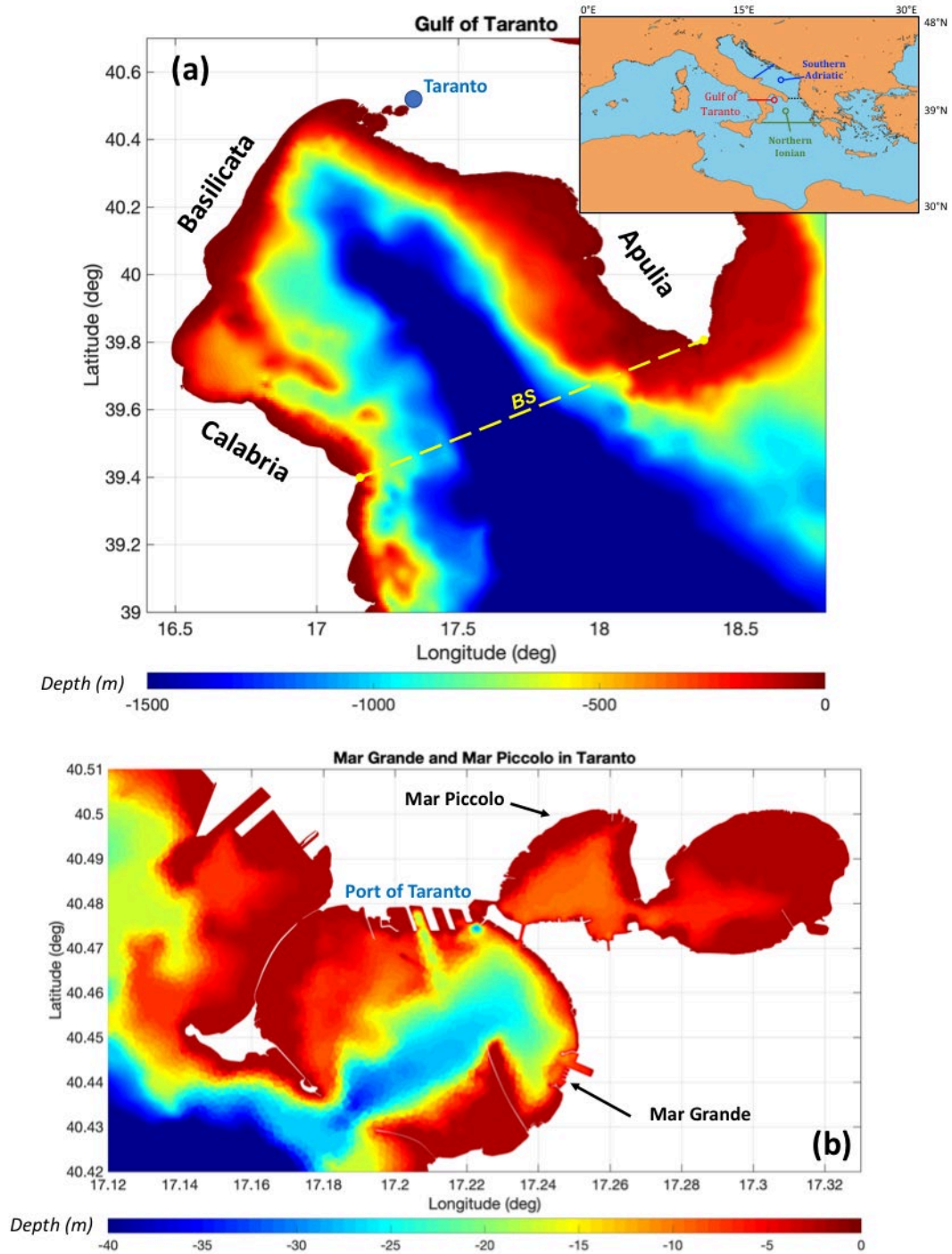


Figure 1. Area of interest: bathymetry and coastline of Gulf of Taranto (a) and Mar Grande (southwestern part of domain, where port of Taranto is located) and Mar Piccolo (northeastern part of domain) of Taranto (b)

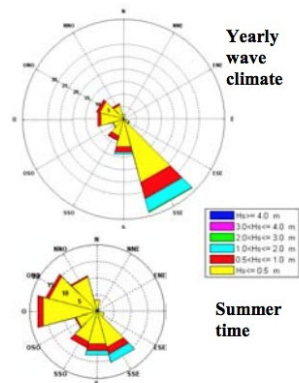


Figure 2. Mean wave climate for the Gulf of Taranto at yearly time-scale for the whole 2006 (top wave rose) and for seasonal time-scale (Summer 2006) from Damiani et al., 2007.

## 2.2. Barcelona

In particular, this work focuses on the coastal waters and port of Barcelona's city in the Northwestern Mediterranean (see Figure 3), where general circulation pattern presents a relatively complex pattern primarily determined by the bottom bathymetry (Sánchez-Arcilla and Simpson, 2002). The characteristics of the continental shelf and the slope are crucial: in the north, the shelf is broad (about 70 km), narrows to less than 20 km in the central stretch of the coast (in front of Barcelona city), and then widens again abruptly to about 60 km further south. The end of the shelf is marked by a reasonably steep slope, with a mean value of about 0.01 km (Mestres et al., 2016). Due to the microtidal character of the Mediterranean Sea, tidal perturbations to the currents are not significant in this area (Poulain et al., 2013; Tsimplis et al., 1995).

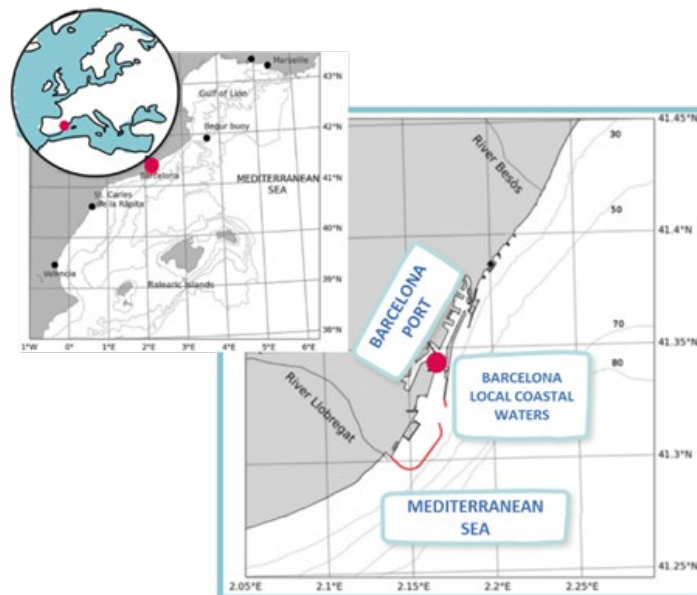


Figure 3. (Left corner) Extended study area comprising the NW Mediterranean. Focus is placed around the Barcelona local coastal waters and port area. Isobaths are drawn up to 80m.

## 3. Methodology

### 3.1. Numerical models

#### Taranto

The modelling system is based on WAVEWATCH III™, a community wave modeling framework that includes the latest scientific advancements in the field of wind-wave modeling and dynamics.

The core of the framework consists of the WAVEWATCH III third-generation wave model, developed at the US National Centers for Environmental Prediction (NOAA/NCEP) in the spirit of the WAM model (Komen et al., 1984).

WAVEWATCH III, hereafter WW3 solves the random phase spectral action density balance equation for wavenumber-direction spectra. The implicit assumption of this equation is that properties of medium (water depth and current) as well as the wave field itself vary on time and space scales that are much larger than the variation scales of a single wave. The model includes options for shallow-water (surf zone) applications, as well as wetting and drying of grid points. Propagation of a wave spectrum can be solved using regular (rectilinear or curvilinear) and unstructured (triangular) grids, individually or combined into multi-grid mosaics.

Source terms for physical processes include parameterizations for wave growth due to the actions of wind, exact and parametrized forms accounting for nonlinear resonant wave-wave interactions, scattering due to wave-bottom interactions, triad interactions, and dissipation due to whitecapping, bottom friction, surf-breaking, and interactions with mud and ice. The model includes several alleviation methods for the Garden Sprinkler Effect, and computes other transformation processes such as the effects of surface currents to wind and wave fields, and sub-grid blocking due to unresolved islands.

Wave energy spectra are discretized using a constant directional increment (covering all directions), and a spatially varying wavenumber grid. First-, second- and third-order accurate numerical schemes are available to describe wave propagation. Source terms are integrated in time using a dynamically adjusted time stepping algorithm, which concentrates computational efforts in conditions with rapid spectral changes.

The model is used worldwide by several institutions to simulate waves of several systems in many regions of the world, from global to coastal scale.

The modelling approach is based on the downscaling of CMEMS Marine products released at the regional scale of Mediterranean Sea. The current Med\_Waves-CMEMS (Korres et al., 2021) implementation is based on WAM Cycle 4.6.2 with proper tuning and maximum spectral steepness limitation and it has been developed as a nested sequence of two computational grids (coarse and fine) to ensure that swell propagating from the North Atlantic towards the strait of Gibraltar is correctly entering the Mediterranean Sea. The coarse grid covers the North Atlantic Ocean from 75°W to 10°E and from 70°N to 10°S in 1/6° resolution while the nested fine grid covers the Mediterranean Sea from 18.125°W to 36.2917°E and from 30.1875°N to 45.9792°N with a 1/24° (~4.6km) resolution. The Med-Waves modelling system resolves the prognostic part of the wave spectrum with 24 directional and 32 logarithmically distributed frequency bins

and the model solutions are corrected by an optimal interpolation data assimilation scheme of along-track significant satellite wave height observations. The system provides a Mediterranean wave analysis and 10 days Mediterranean wave forecasts updated twice a day.

### Barcelona

Reliable knowledge on surface gravity waves, currents, and their interactions in the ocean is of great importance to many applications, such as weather forecasting, search and rescue, beach erosion, and site selections for offshore infrastructures (Hashemi and Neill, 2014). Waves and currents form a complex system usually discussed, assuming the influence of waves on hydrodynamics and the impact of currents on waves distinctly (Benetazzo et al., 2013). This broad topic is usually referred to with the general term of Wave–Current Interaction (WCI) that, from the general point of view, traces back to the theoretical works of Longuet-Higgins (1964) on longshore currents flows produced by waves, and to the studies of the dynamics of waves in a moving medium (Tayfun et al., 1976). Physically, ocean currents can modify the relative speed of the air above the sea surface (relative wind effect) and change the absolute frequency of waves known as the Doppler shift. In addition, spatial variability of currents can modify the relative wave frequency and cause wave refraction, shoaling, and breaking that mimic bathymetric effects (Ding and Wang, 2011). The surface gravity waves, in return, can affect vertical mixing, surface and bottom stress experienced by currents. The surface waves and currents can also exchange energy through the concept of radiation stress (Stewart et al., 1974; Mellor, 2003) or vortex force (McWilliams et al., 2004; Ardhuin et al., 2008).

In the framework of the EuroSea initiative, the LIM-UPC team is developing a 3D hydrodynamic tool with enough resolution to solve the inner dynamics of local domains such as Barcelona's coastal waters, harbor, and beaches. The effect on waves of the Wave-Current Interaction (WCI) process in Barcelona's coastal waters and the port is investigated using the Coupled Ocean-Atmosphere-Wave-Sediment Transport (COAWST) modeling system. COAWST relies on the ocean model ROMS (Regional Ocean Modeling System) and SWAN (Simulating WAVes Nearshore) wave model. The simulations are based on a two-way coupling between ROMS and SWAN running on the same computational grids. The atmospheric forcing was uncoupled, and CMEMS products provided fields.

### *Circulation model:*

ROMS is a three-dimensional, free-surface, topography-following numerical model that solves finite difference approximations of Reynolds Averaged Navier Stokes (RANS) equations using hydrostatic and Boussinesq approximations with a split-explicit time-stepping algorithm (Shchepetkin and McWilliams, 2005; Haidvogel et al., 2008; Shchepetkin and McWilliams, 2009). In addition, ROMS includes options for various model components such as different advection schemes (second, third, and fourth-order), turbulence closure models (e.g., Generic Length Scale mixing, Mellor-Yamada, Brunt-Väisälä frequency mixing, user-provided analytical expressions, K-profile parameterization), and several options for boundary conditions.

We used the latest version of the ROMS model (version 3.9) at the date of publication of this deliverable. However, numerical details and a complete model description, user documentation, and source code are available at the ROMS website<sup>1</sup> for future checks and improvements.

---

<sup>1</sup> <http://www.myroms.org/>



### *Wave model*

SWAN is a state-of-the-art 3rd generation spectral wave model which computes random, short-crested wind-generated waves in offshore and coastal regions. The model describes the generation, evolution, and dissipation of the wave action density spectrum  $N$  (space, time;  $\sigma$ ,  $\theta$ ), where  $\theta$  is the wave propagation direction, and  $\sigma$  is the wave relative frequency. SWAN solves a radiative time-dependent transport equation in the variable  $N$ , accounting for the wind input, the wave-wave interactions, and the dissipation terms in deep and shallow waters. The ambient current affects the density spectrum balance in two ways. One way is that  $N$  will be propagated with a velocity modified by the local ocean current. A second way is that the effects of ocean currents are accounted for by using the apparent local wind speed and direction to modify the wind stress (Kara et al., 2007). The wind speed modification by the local currents is implemented in COAWST, assuming the atmosphere flow relative to a moving frame: the wind speed is shifted by the ocean current velocity (validations and limits provided by Hersbach and Bidlot, 2008).

We used the latest version of the SWAN model (version 41.31) at the date of publication of this deliverable. However, numerical details and a complete model description, user documentation, and source code are available at the SWAN website<sup>2</sup> for future checks and improvements.

### *Coupling tool*

The COAWST model utilizes the model-coupling toolkit (MCT) to achieve communication among the submodels via the message passing interface (Jacob et al., 2005). In the coupling process, ROMS receives the surface and bottom wave direction, height, length, period, percentage breaking, energy dissipation, and bottom orbital velocity from SWAN, while it provides bathymetry, bottom elevation, sea-surface height, and depth-averaged currents to SWAN.

We used the latest version of the COAWST modeling system (version 3.7) at the date of publication of this deliverable. However, complete model details are available on the COAWST website<sup>3</sup> for detailed checks and future improvements.

## 3.2. Grid generation and bathymetry interpolation

### Taranto

In EuroSea, we have developed a specific and hyper-resolution configuration for Taranto Seas, hereafter GT-WAVE. The new system covers only the GT with a horizontal resolution from 3 km in open-sea to 100 m in the coastal waters to 20 m in the port of Taranto. Figure 4 shows the grid and bathymetry in GT and MG-MP. A single open boundary is created connecting Calabria and Apulia coasts through the GT-BS (see Figure 1a). This configuration has been created to perform specific process studies and long-term hindcast simulations, due to the reduced density meshes in respect with the first one. The new horizontal grid has been created adopting advanced and customized tools (mainly python-based) of meshing based on GMSH<sup>4</sup> and BLENDER<sup>5</sup> software.

The bathymetry was derived from the EMODnet<sup>6</sup> product at a resolution of  $1/8 \times 1/8$  arc-minutes (circa 230 x 230 meter), resolution for open sea and coastal waters and integrated with higher-resolution bathymetry

---

<sup>2</sup> <https://swanmodel.sourceforge.io/>

<sup>3</sup> <https://www.usgs.gov/software/coupled-ocean-atmosphere-wave-sediment-transport-coawst-modeling-system>

<sup>4</sup> <http://gmsh.info/>

<sup>5</sup> <https://www.blender.org/>

<sup>6</sup> <https://www.emodnet-bathymetry.eu/>

(resolutions of order of meter) for coastal areas in MG-MP and Taranto Port area provided by the Italian Navy Hydrographic Institute. The wave spectra have been discretized in 24 directions (covering the full circle) and 32 frequencies, from 0.05 Hz to 0.9597 Hz.

#### Barcelona

Bathymetries are built using a combination of bathymetric data from EMODnet<sup>7</sup> and specific high-resolution sources provided by local Port Authorities. An updated and higher resolution bathymetry is also applied to adjust the open boundary to the coastal bathymetries in the port domains. Finally, the bathymetry information interpolated is smoothed using a Shapiro filter with an r-factor criterion below 0.25.

The bottom boundary layer was parameterized with a logarithmic profile using a characteristic bottom roughness height of 0.002 m. The turbulence closure scheme for the vertical mixing is the generic length scale (GLS) tuned to behave as k-epsilon (Warner et al., 2005). Horizontal harmonic mixing of momentum is defined with constant values of  $5 \text{ m}^2\text{s}^{-1}$ .

### 3.3. Initial and Lateral boundary conditions. Forcings.

#### Taranto

The modelling system is downscaled from Med-Waves-CMEMS in term of open boundaries. The scalar fields from Med-Waves-CMEMS (significant wave surface height, peak wave period and mean direction) are treated at the boundary nodes of the nested system through the Yamaguchi, 1984 approximation, to rebuild local wave spectra.

The model is initialized using the fetch limited approach: the local JONSWAP spectrum is calculated using the local wind speed and direction, using the spatial grid size as fetch.

Meridional and zonal 10 m wind components (U10M and V10M) of well-consolidated atmospheric products from ECMWF (6.5 km resolution and 3h frequency) are adopted as forcing. The atmospheric fields are corrected by land-contaminated points following Kara et al. (2007) and horizontally interpolated at each ocean grid node by means of linear interpolation.

#### Barcelona

The model configuration is nested into the daily updated regional ocean forecast products delivered by CMEMS- IBI (Sotillo et al., 2015). At the sea surface, the models are driven by high frequency (hourly) wind stress, atmospheric pressure, and fluxes of water and surface heat derived from the Spanish Meteorological Agency (AEMET) forecast services, based on two operational applications of the HIRLAM (High-Resolution Limited Area Model) model: one, the HNR application which is corresponded with the Iberic Peninsula geographic domain (0.05° resolution and a forecast horizon of + 36 h) and the ONR application which is corresponded with the Euro-Atlantic geographic domain (0.16° resolution and a forecast horizon of + 72 h). Further detailed information on this methodology can be found in Sotillo et al. 2019.

The HNR and ONR fields are jointly used according to the best available basis and pre-processed to obtain wind surface stress, surface net heat, and salinity fluxes. Hourly barotropic water currents and sea level are provided by CMEMS-IBI and consistently applied as Open Boundary Conditions (OBC) with Chapman and Flather algorithms (Carter and Merrifield 2007). Moreover, daily average values of CMEMS-IBI currents,

---

<sup>7</sup> <https://emodnet.ec.europa.eu>

temperature, and salinity are imposed through the water column as clamped (Dirichlet) boundary conditions (Sotillo et al., 2019).

### 3.4. Physical and numerical setting

#### Taranto

GT\_WAVE has been implemented following WAM Cycle4 model physics (Günther et al. 1992). The propagation scheme used is a third order scheme (Ultimate Quickest) with "Garden Sprinkler Effect" alleviation method of spatial averaging. Wind input and dissipation are based on Ardhuin et al., 2010, in which the wind input parametrization is adapted from Janssen's quasi-linear theory of wind-wave generation (Janssen, 1991, Chalikov and Belevich, 1993), following adjustments performed by Bidlot et al. 2005 and Bidlot 2008. Nonlinear wave-wave interaction have been modelled using the Discrete Interaction Approximation (DIA) (Hasselmann et al. 1986, Hasselmann et al. 1985).

The model system includes shallow water physics for coastal processes. Nonlinear triad interactions are modelled using the LTA model of Eldeberky (1996). Depth-induced breaking has been implemented using the approach of Battjes and Janssen (1978).

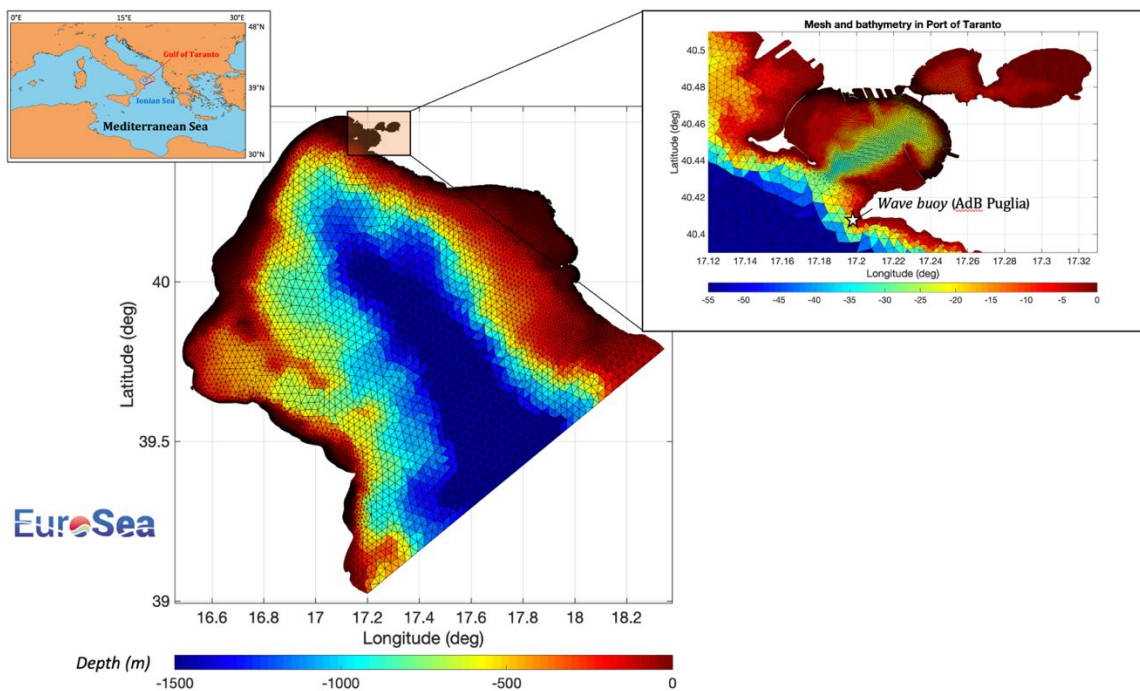


Figure 4. Horizontal grid with bathymetry overlapped for Gulf of Taranto system and for MG-MP. Star symbol indicates the wave buoy location (property of Autorità di Bacino, Apulia region) used for validation.

#### Barcelona

The numerical simulations are performed on two-nested grids configurations (see Figure 5). The model is performed on two-nested grids configurations with two-way ocean refinement and one-way wave refinement with coupled exchanges between two grids for the fields of currents, bathymetry from the ocean to the wave, and wave dissipation, height, length, and direction, surface and bottom periods, and bottom orbital velocities from the wave to the ocean model (see Figure 5).

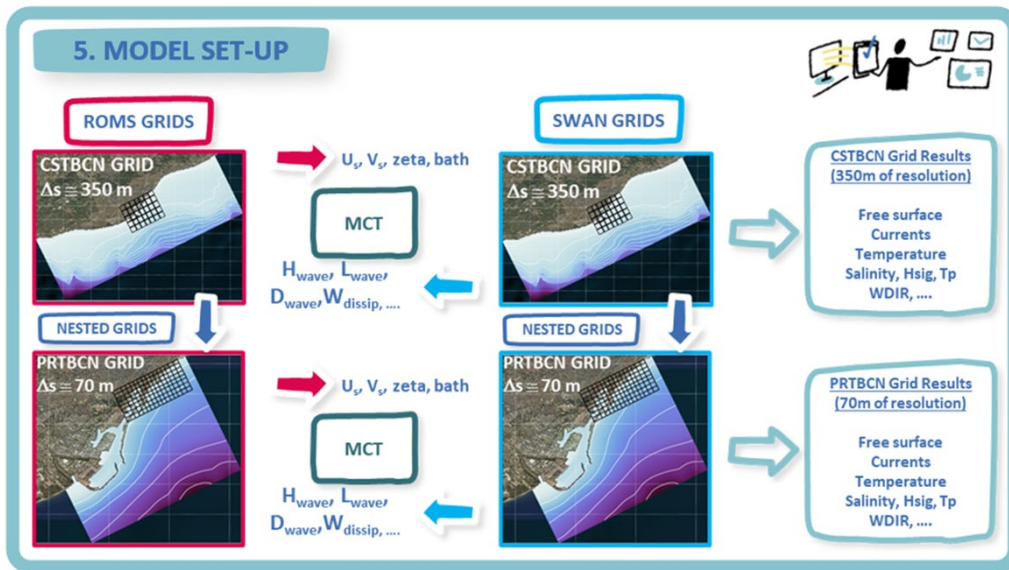


Figure 5. Setup configuration to the operational model scheme.

### 3.5. Results

#### Taranto

Here we show results in the coastal and harbour scale of Taranto and a quantitative analysis comparing the modelling results with observations, especially during extreme wave events.

Figure 6 shows Significant Wave Height (Hs) over the entire model domain under downwind conditions (Easterly winds), with a zoom on the MG.

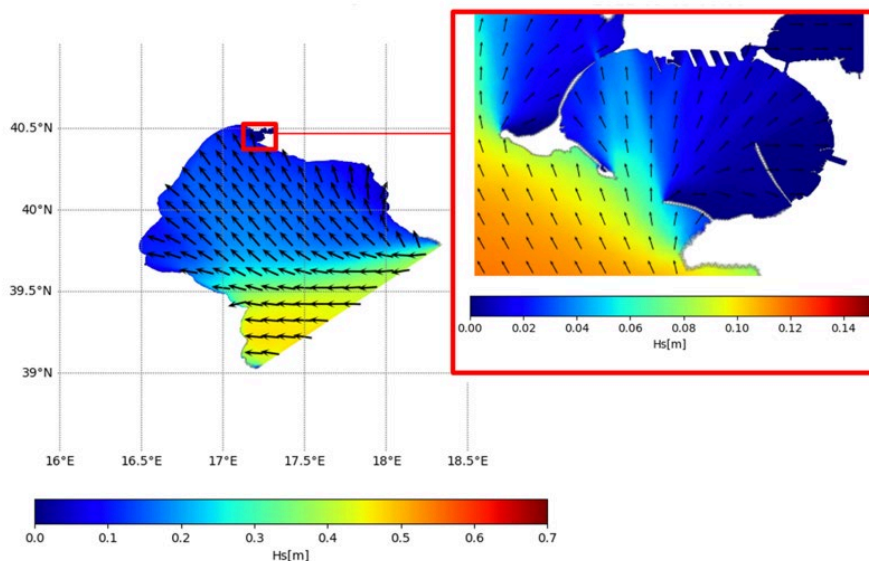


Figure 6. Significant wave height on the Gulf of Taranto (left panel) and on the MG (right panel) under downwind condition.

Figure 7 shows a numerical experiment aimed to assess the impact on Hs and mean wave period (Tm) due the inclusion of shallow water physics in GT\_WAVE. The top panels show the Hs and Tm for the full set-up

(both deep and shallow water physics), while the bottom panel the difference between simulation using the full set-up and simulation based on only deep-water physics. In particular the Hs of full set-up is comparable to the one of only deep water set-up except for the coast, where shallow water physics are activated. The Hs reduction in full set-up experiment is estimated to be around  $\sim -15\%$  close to the Isola di San Pietro coast. Similar behavior is reported for Tm.

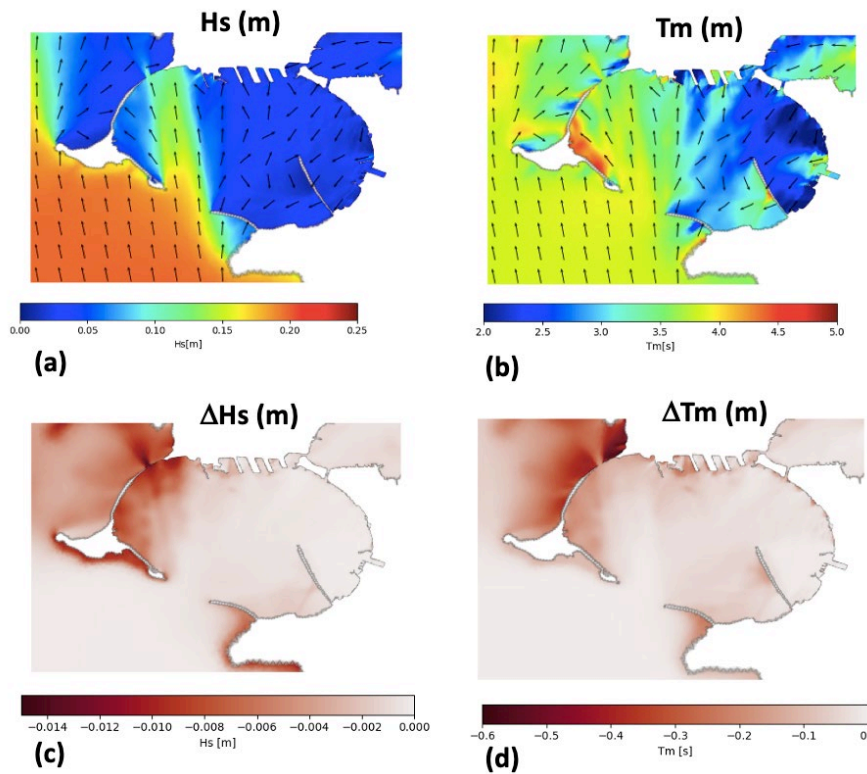


Figure 7. Significant wave height (a) and mean period (b) for GT-WAVE full set-up (both deep and shallow water physics). Difference between full set-up and only deep-water physics for significant wave height (c) and mean period (d).

In the next section we analyzed and validated the GT-WAVE implementation, considering three extreme events between 2014 and 2016, where data from buoys are available. The wave buoy data have been provided by the Autorità di Bacino of Apulia region, and they were compared to Hs and Tm of GT-WAVE and its parent model (Med-Waves-CMEMS). The water depth where the buoy is located approximately at 72 m, thus we were able to validate only the deep-water physics of our implementation. The location of the buoy is reported in Figure 4.

The first event occurred on 2014, on 4-6 October. In Figure 8 we report the significant wave map at the highest peak of the event and the timeseries of Hs and Tm during the event. Two peaks of Hs (1.8m and 1.6m) are present, with a mean direction at boundary from southeast. Both the peaks were better represented by GT-WAVE with respect to the CMEMS parent model. For the first peak it is evident an underestimation by both the models, while the second one is very well described by GT-WAVE while CMEMS underestimates it. Considering the wave period, CMEMS showed a significant underestimation. GT-WAVE performs better reducing the underestimation of 50%.

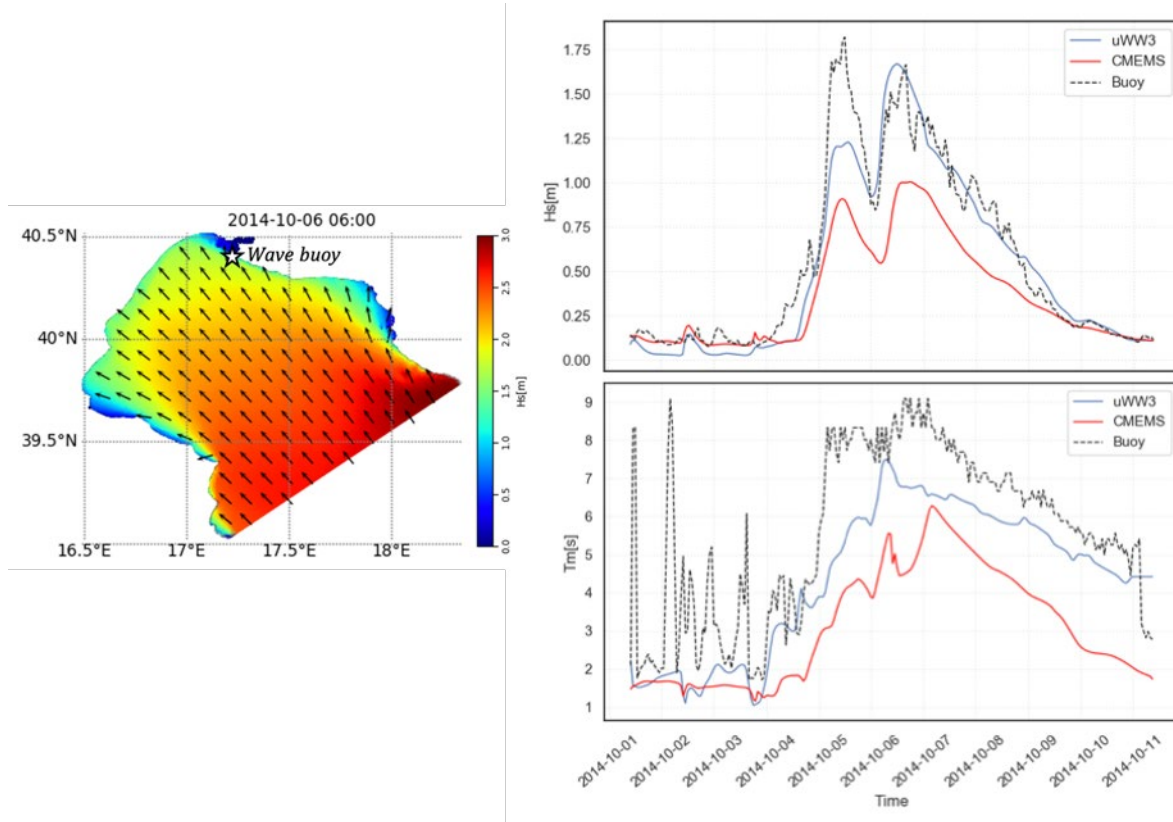


Figure 8. Map of Hs at the peak of the event of October 2014. Models (GT-WAVE and Med-Waves-CMEMS) timeseries of Hs and Tm compared with wave buoy observations.

During the second event, occurred in the middle of February 2015, the waves entered the open boundary from South. In Figure 9 we report the significant wave map at the highest peak of the event and the timeseries of Hs and Tm during the event. Also for this case, the event showed 2 peaks respectively on 17<sup>th</sup> and 23<sup>th</sup> of February. The first peak, the lowest, reached approximately 2m of Hs, and it was well represented by GT-WAVES. After that, the sea-state restoring phase showed an overestimation of Hs in GT-WAVES, and Hs was better described by CMEMS. The second peak can be considered a real extreme event, with Hs exceeding 3.5m. The event is slightly better described by CMEMS. It is evident that CMEMS tends to underestimated Hs and GT-WAVE tends to overestimate it. The wave period of CMEMS showed a net underestimation, while GT-WAVE is closer to the observed data.

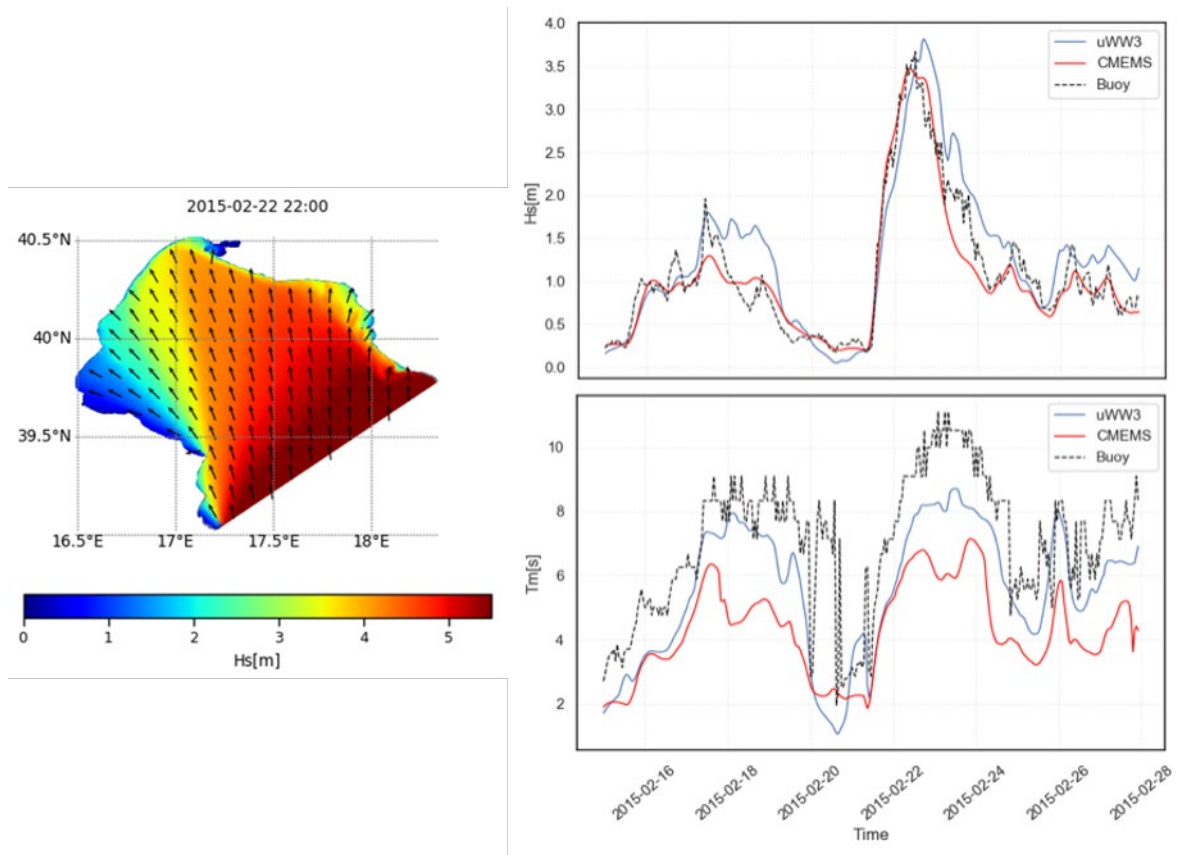


Figure 9. Map of Hs at the peak of the event of February 2015. Models (GT-WAVE and Med-Waves-CMEMS) timeseries of Hs and Tm compared with wave buoy observations.

The third event occurred in March 2016. In Figure 10 we report the significant wave map at the highest peak of the event and the timeseries of Hs and Tm during the event. During the event two peaks of Hs are present, respectively on 13<sup>th</sup> and 17<sup>th</sup> of March 2016. The wave direction approaching to the open boundary was S-SE oriented. The first peak (~2.1m) was underestimated by CMEMS, while better represented by GT-WAVE. The second peak (~3.8m) was underestimated by both the models even if GT-WAVE (~3.1m) was closer to observations than CMEMS (~2.8m). Unfortunately, the observation was not complete because of lacking buoy data on 18<sup>th</sup> of March. Again, for the mean period the tendency of the previous plots, with both models underestimating the observations, but higher accuracy of GT-WAVE, is confirmed.

We can conclude that GT-WAVE generally performs better than CMEMS for these specific events and in the area. In addition, we would like to stress that the CMEMS model is also equipped with satellite wave assimilation, while no assimilation is included in the GT-WAVE model.

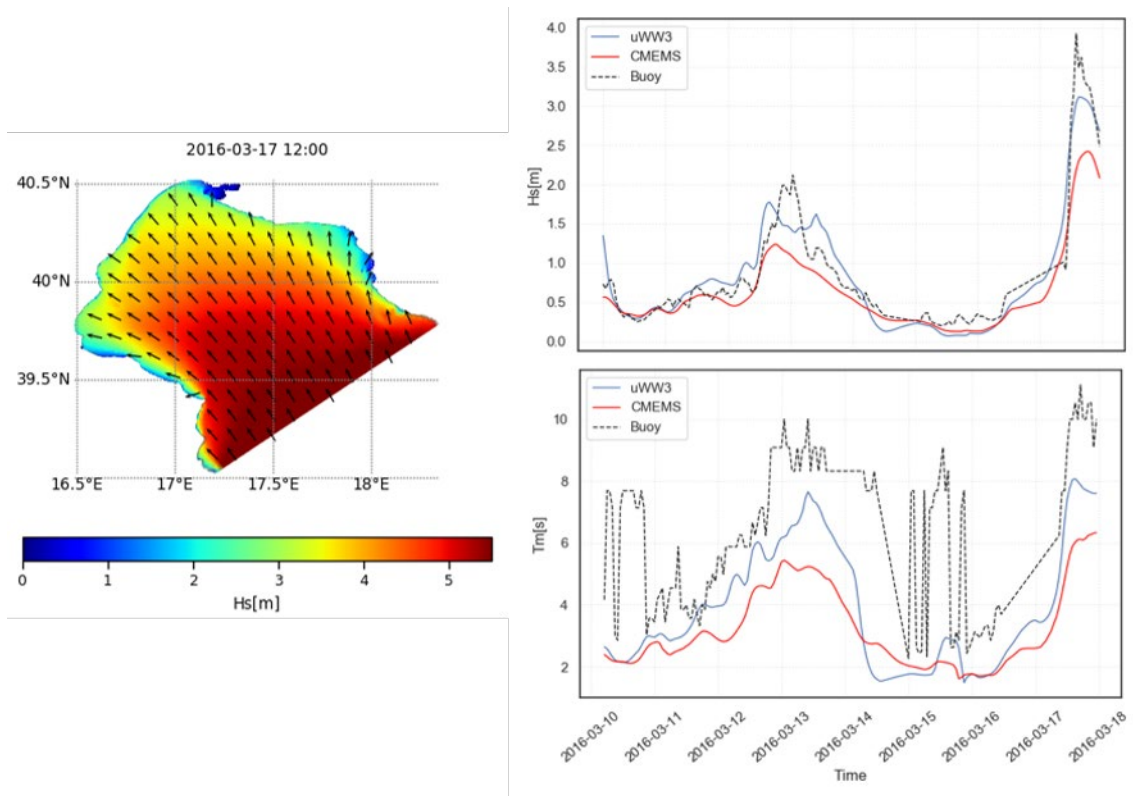


Figure 10. Comparison between wave buoy observations, GT\_WAVE and Med-Waves-CMEMS during the extreme events occurred in the middle of March 2016.

## Barcelona

The model simulation generates three-day forecasts of three-dimensional waves heights fields and other oceanographic variables, such as wave direction, wave period, current fields, temperature, salinity, and sea level. Product quality assessment is a crucial issue for operational forecast systems (Sotillo et al., 2019). For that reason, the model outputs are being validated with in-situ observations from field campaign data; preliminary validations display good agreements and correlations between them, allowing us to understand better the quality and accuracy of the model products (Figure 11). However, there is still necessary work in the wave model operational implementation to generate forecast model products.



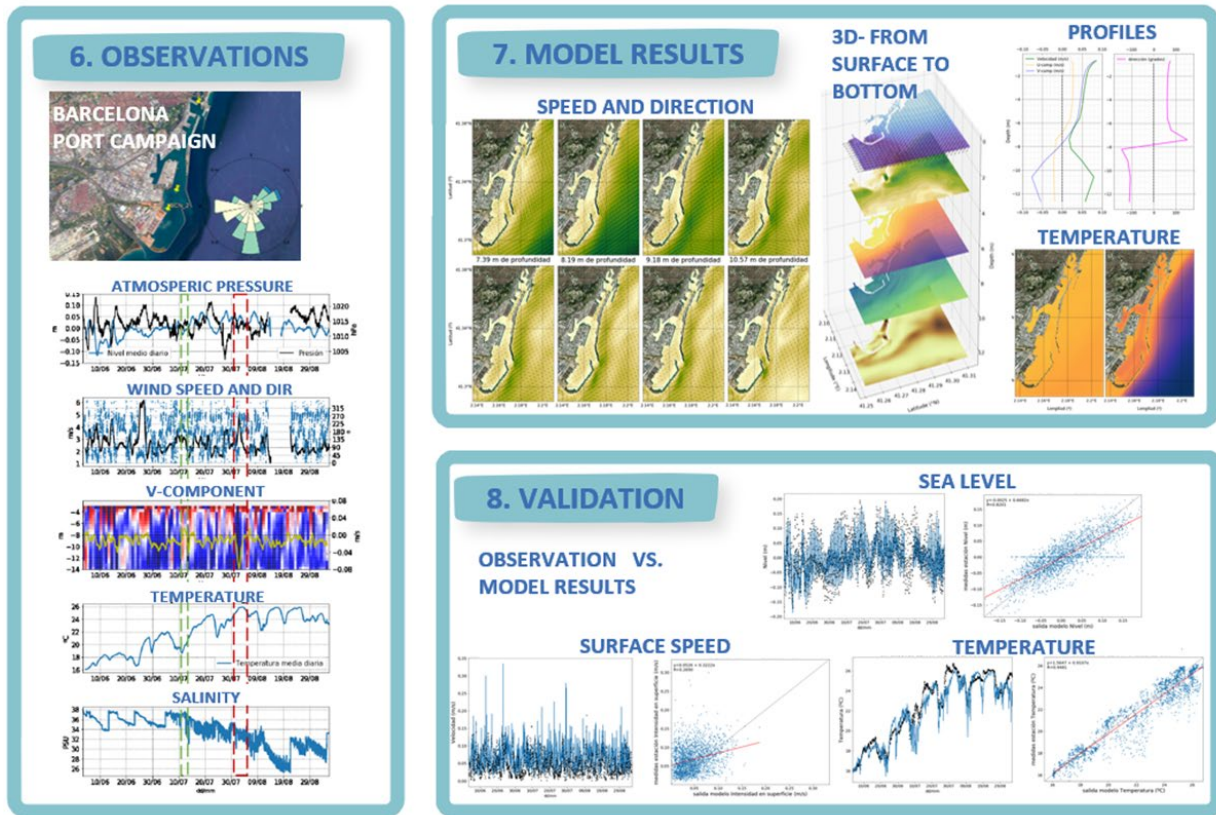


Figure 11. Overview of the observations (left panel), model results (upper right panel), and validation (lower right panel) at Barcelona's local coastal waters and port.

Throughout the Barcelona port campaign, two main patterns were identified: the water entered through the port's mouth from the outside to the interior of the port (entry episode) and another where the water left through the port's mouth into local coastal waters (exit episode). Figure 12 and Figure 13 show some oceanographic variables modeled from these episodes (Figure 12 shows an entry episode, and Figure 13 shows an exit episode). Figure 12 and Figure 13 also show surface speed, direction, temperature, and sea-level correlations between modeled variables and Barcelona's port campaign measurements.

Regarding correlations, the model predicts well the Sea-level. The correlation is 0.82. Respecting the surface temperature, the correlation between predictions and observations is 0.95. Concerning current surface speed and direction, the model underpredicts the observations, and the correlations between modeled values and measurements are 0.27-0.35. The new improvements in future coupled model versions will try to improve the correlations between the model predictions and the observations.

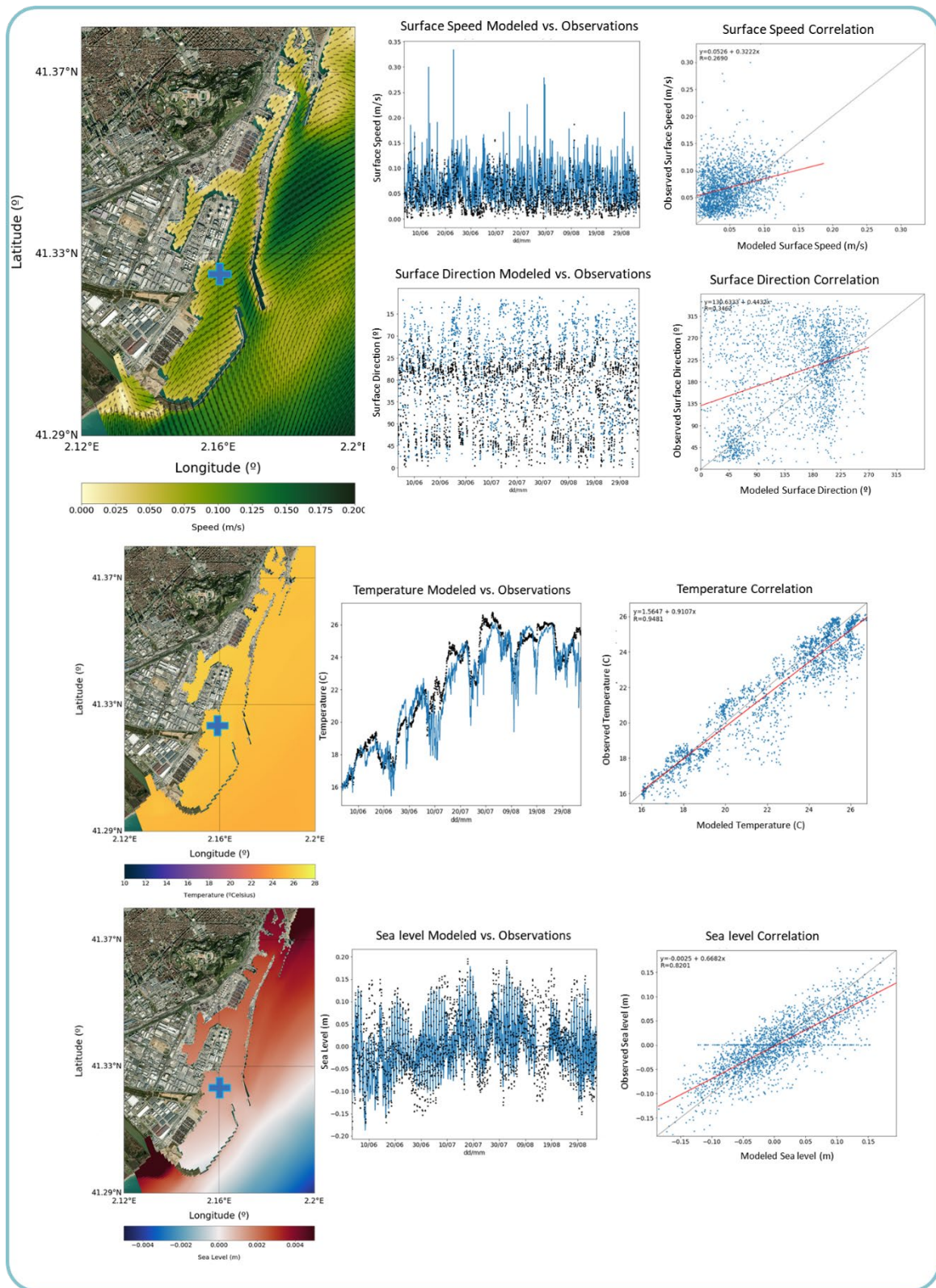


Figure 12. Surface Speed (m/s), Direction (°), Temperature (° Celsius), and Sea level (m) modeled results versus observations from Barcelona's port campaign during an entry water episode.

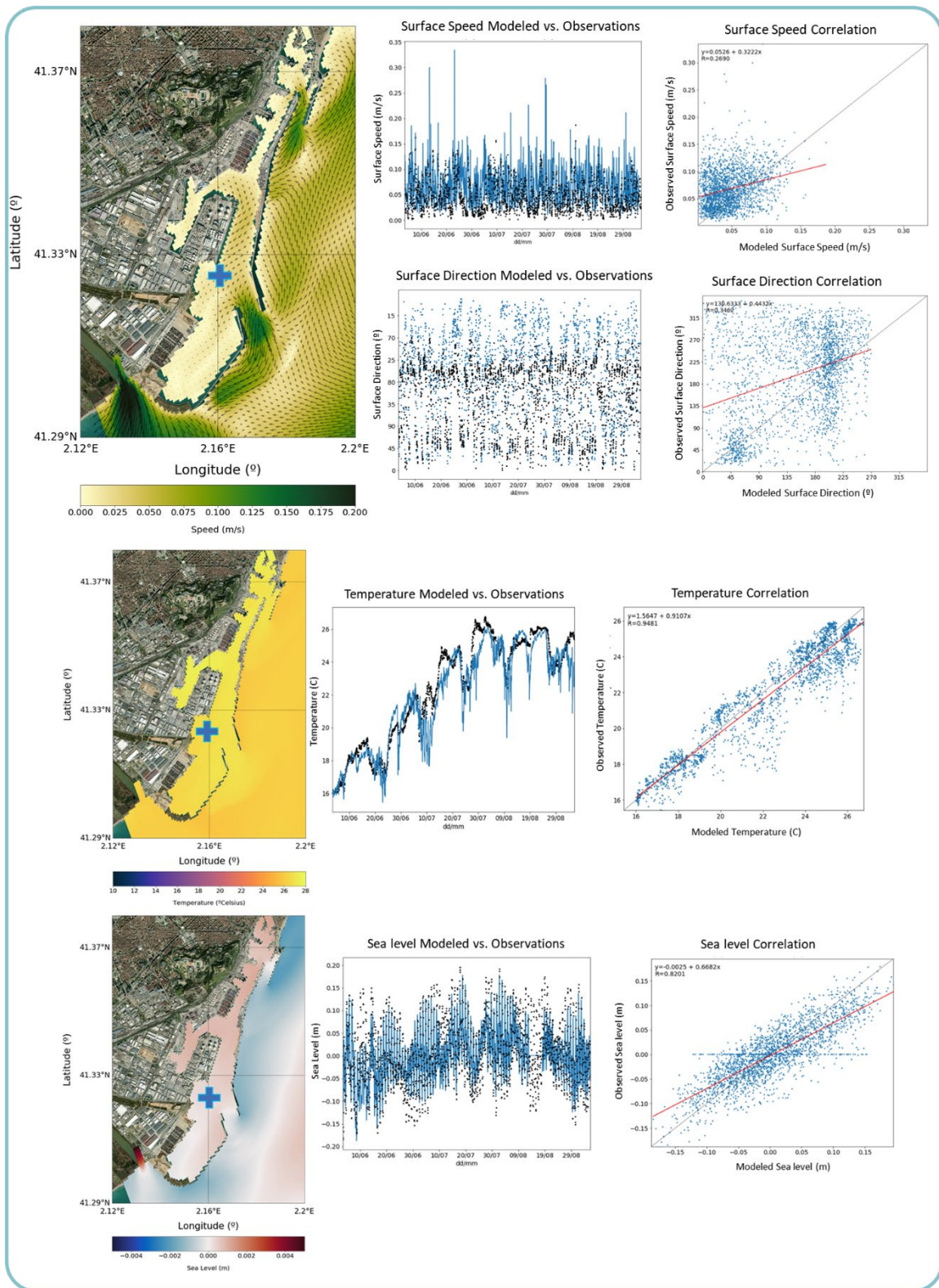


Figure 13. Surface Speed (m/s), Direction (°), Temperature (°Celsius), and Sea level (m) modeled results versus observations from Barcelona's port campaign during an exit water episode.

## References

### References for Taranto subsections

- Ardhuin, F.; Rogers, E.; Babanin, A.V.; Filipot, J.F.; Magne, R.; Roland, A.; Collard, F. Semiempirical dissipation source functions for ocean waves. Part I: Definition, calibration, and validation. *J. Phys. Oceanogr.* 2010, 40, 1917–1941.
- Battjes, J. A., and J. P. F. M. Janssen (1978), Energy loss and set-up due to breaking of random waves, in Proc. 16th Int. Conf. Coastal Eng., pp. 569–587, ASCE.
- Bidlot, J, S Abdalla, and PAEM Janssen (2005). A revised formulation for ocean wave dissipation in CY25R1. In: Internal Memorandum Research Department
- Bidlot, JR (2008). Intercomparison of operational wave forecasting systems against buoys: Data from ECMWF, MetO
- Chalikov, D. V., and M. Y. Belevich (1993), One-dimensional theory of the wave boundary layer, *Bound. Layer Meteor.*, 63, 65–96.
- Damiani, L., Bruno, M.F., Molfetta, M.G.. "Coastal zone monitoring in Apulia region: first analysis on meteomarine climate." *Proceedings of the 5th International Symposium on Environmental Hydraulics (ISEH 2007)*, Tempe, AZ, USA. 2007.
- Eldeberky, Y. (1996), Nonlinear transformation of wave spectra in the nearshore zone, Ph.D. thesis, Delft University of Technology, Delft, The Netherlands, 203 pp.
- Greco, M., & Martino, G. (2014). Assessment of maritime erosion index for Ionian-Lucanian coast. In *Engineering Geology for Society and Territory—Volume 4* (pp. 41-44). Springer, Cham.
- Hasselmann, S.; Hasselmann, K.; Allender, J.K.; Barnett, T.P. Computations and parameterizations of the nonlinear energy transfer in a gravity-wave spectrum. Part II: Parameterizations of the nonlinear energy transfer for application in wave models. *J. Phys. Oceanogr.* 1985, 15, 1378–1391.
- Hasselmann, D.; Bösenberg, J.; Dunkel, M.; Richter, K.; Grünwald, M.; Carlson, C. Measurements of wave-induced pressure over surface gravity waves. In *Wave Dynamics and Radio Probing of the Ocean Surface*; Springer: Boston, MA, USA, 1986; pp. 353–368.
- Janssen, P. A. E. M. (1991), Quasi-linear theory of of wind wave generation applied to wave forecasting, *J. Phys. Oceanogr.*, 21, 1,631–1,642.
- Kara, B. A., Wallcraft, A. J., Hurlburt, H. E., 2007. A Correction for Land Contamination of Atmospheric Variables near Land–Sea Boundaries, *J. Phys. Oceanogr.*, 37, 803–818.
- Komen, G. J., S. Hasselmann and K. Hasselmann, 1984: On the existence of a fully developed wind-sea spectrum. *J. Phys. Oceanogr.*, 14, 1,271–1,285.
- Korres, G., Ravdas, M., Zacharioudaki, A., Denaxa, D., & Sotiropoulou, M. (2021). Mediterranean Sea Waves Analysis and Forecast (CMEMS MED-Waves, MedWAM3 system) (Version 1) set. Copernicus Monitoring Environment Marine Service (CMEMS).  
[https://doi.org/10.25423/CMCC/MEDSEA\\_ANALYSISFORECAST\\_WAV\\_006\\_017\\_MEDWAM3](https://doi.org/10.25423/CMCC/MEDSEA_ANALYSISFORECAST_WAV_006_017_MEDWAM3)

Liste, M., Mestres, M., Espino, M., Sanchez-Arcilla, A., García-León, M., G. Sotillo, M., and Alvarez-Fanjul, E. (2021). High-Resolution 3D Forecasting System for Barcelona's Beaches and Coastal Waters. EGU General Assembly. 19-30 April 2021. Vienna, Austria.

Mesinger, F., Janjic, Z. I., Nickovic, S., Gavrilov, D., Deaven, D.G., 1988. The step-mountain coordinate: model description and performance for cases of Alpine lee cyclogenesis and for a case of an Appalachian redevelopment, *Mon. Weather Rev.*, 116, 1493–1518.

Pinardi, N., Lyubartsev, V., Cardellicchio, N., Caporale, C., Ciliberti, S., Coppini, G., De Pascalis, F., D'Alti, L., Federico, I., Filippone, M., Grandi, A., Guideri, M., Lecci, R., Lamberti, L., Lorenzetti, G., Lusiani, P., Macripo, C. D., Maicu, F., Mossa, M., Tartarini, D., Trotta, F., Umgiesser, G., Zaggia, L., 2016. Marine Rapid Environmental Assessment in the Gulf of Taranto: a multiscale approach, *Nat. Hazards Earth Syst. Sci.*, 16, 2623–2639

Yamaguchi, M. (1984). Approximate expressions for integral properties of the JONSWAP spectrum. *Doboku Gakkai Ronbunshu*, 1984(345), 149-152.

#### References for Barcelona subsections

Ardhuin, F., N. Raschle, and K. Belibassakis (2008), Explicit wave-averaged primitive equations using a generalized Lagrangian mean, *Ocean Modell.*, 20, 35–60, <https://doi.org/10.1016/j.ocemod.2007.07.001>.

Benetazzo, A., Carniel, S., Scavo, M., Bergamasco, A. (2013). Wave–current interaction: Effect on the wave field in a semi-enclosed basin. *Ocean Modelling* 70 (2013) 152–165.

Ding, Y., and Wang, S.Y. (2011). Modeling of Wave-Current Interaction Using a Multidirectional Wave Action Balance Equation. *Coastal Engineering Proceedings*. <https://doi.org/10.9753/icce.v32.waves.47>.

Haidvogel, D. B., Arango, H.G., Budgell, W. P., Cornuelle, B. D., Curchitser, E., Di Lorenzo, E., Fennel, K., Geyer, W. R., Hermann, A. J., Lanerolle, L., Levin, J., McWilliams, J. C., Miller, A. J., Moore, A. M., Powell, T. M., Shchepetkin, A. F., Sherwood, C. R., Signell, R. P., Warner, J. C., Wilkin, J. (2008). Ocean forecasting in terrain-following coordinates: Formulation and skill assessment of the Regional Ocean Modeling System, *Journal of Computational Physics*. 227, 3595-3624.

Hashemi, M., and S. Neill (2014), The role of tides in shelf-scale simulations of the wave energy resource, *Renewable Energy*, 69, 300–310, <https://doi.org/10.1016/j.renene.2014.03.052>.

Hersbach, H., Bidlot, J.-R. 2008. The relevance of ocean surface current in the ECMWF analysis and forecast system. In: *Workshop on Ocean-Atmosphere Interactions*, Reading, United Kingdom, European Centre for Medium-Range Weather Forecasts, pp. 61–73.

R. Jacob, J. Larson, and E. Ong, "M×N communication and parallel interpolation in community climate system model version 3 using the model coupling toolkit," *The International Journal of High Performance Computing Applications*, vol. 19, no. 3, pp. 277–292, 2005.

Longuet-Higgins, M., and R. Stewart (1964), Radiation stresses in water waves; a physical discussion, with applications, *Deep Sea Res. Oceanogr. Abstr.*, 11, 529–562, [https://doi.org/10.1016/0011-7471\(64\)90001-4](https://doi.org/10.1016/0011-7471(64)90001-4).

McWilliams, J., J. Restrepo, and E. Lane (2004), An asymptotic theory for the interaction of waves and currents in coastal waters, *J. Fluid Mech.*, 511, 135–178, <https://doi.org/10.1017/S0022112004009358>.

Mellor, G. L. (2003), The three-dimensional current and surface wave equations. *J. Phys. Oceanogr.*, 33, 1978–1989.

Mestres M, Grifoll M, Sánchez-Arcilla A. 2016. Analysis of current intensification in the Northwest Mediterranean shelf. *Cont Shelf Res.* 114:29–40. ISSN 0278-4343, <https://doi.org/10.1016/j.csr.2015.12.011>.

Poulain, P.-M., Bussani, A., Gerin, R., Jungwirth, R., Mauri, E., Menna, M., Notar-Stefano, G., 2013. Mediterranean surface currents measured with drifters: from basin to subinertial scales. *Oceanography* 26(1), 38–47. <http://dx.doi.org/10.5670/oceanog.2013.03>.

Sánchez-Arcilla, A. and Simpson, J., 2002. The narrow shelf concept: couplings and fluxes. *Cont. Shelf Res.* 22(2), 153–172.

Shchepetkin, A. F., McWilliams, J.C. (2005). The Regional Oceanic Modeling System: A split-explicit, free-surface, topography-following coordinate oceanic model. *Ocean Modeling* 9, 347–404. <https://doi.org/10.1016/j.ocemod.2004.08.002>.

Shchepetkin, A. F., McWilliams, J. C. (2009). Correction and commentary for "Ocean forecasting in terrain-following coordinates: Formulation and skill assessment of the regional ocean modeling system" by Haidvogel et al., *J. Comp. Phys.* 227, pp. 3595–3624." *Journal of Computational Physics.* 228, 8985-9000.

Sotillo, MG., P. Cerralbo, P. Lorente, M. Grifoll, M. Espino, A. Sánchez- Arcilla & E. Álvarez-Fanjul (2019): Coastal ocean forecasting in Spanish ports: the SAMOA operational service, *Journal of Operational Oceanography*, <https://doi.org/10.1080/1755876X.2019.1606765>.

Sotillo MG, Cailleau S, Lorente P, Levier B, Aznar R, Reffray G, AmoBaladrón A, Chanut J, Benkiran M, Alvarez-Fanjul E. 2015. The MyOcean IBI ocean forecast and reanalysis systems: operational products and roadmap to the future Copernicus service. *J Oper Oceanogr.* 8(1):63–79. <https://doi.org/10.1080/1755876X.2015.1014663>.

Stewart, R.H., Joy, J.W., 1974. HF radio measurements of surface currents. *Deep Sea Res. Oceanogr. Abstracts* 21, 1039–1049.

Tayfun, M.A., Dalrymple, R.A., Yang, C.Y., 1976. Random wave–current interactions in water of varying depth. *Ocean Eng.* 3, 403–420.

Tsimplis, M.N., Proctor, R., Flather, R.A., 1995. A two-dimensional tidal model for the Mediterranean Sea. *J. Geophys. Res.* 100 (C8), 16223–16239. <http://dx.doi.org/10.1029/95JC01671>.

Warner JC, Sherwood CR, Arango HG, Signell RP. 2005. Performance of four turbulence closure models implemented using a generic length scale method. *Ocean Model.* 8(1):81–113.